Acta Materialia 135 (2017) 244–251

Contents lists available at ScienceDirect

Acta Materialia

journal homepage: www.elsevier.com/locate/actamat

Full length article

A novel type of Co–Ti–Cr-base γ/γ' superalloys with low mass density

Christopher H. Zenk [a, *], Ivan Povstugar [b], Rui Li [b], Fernando Rinaldi [c], Steffen Neumeier [a], Dierk Raabe [b], Mathias Göken [a]

[a] Friedrich-Alexander-Universität Erlangen-Nürnberg (FAU), Materials Science & Engineering, Institute I, Martensstr. 5, 91058, Erlangen, Germany
[b] Department of Microstructure Physics and Alloy Design, Max-Planck-Institut für Eisenforschung, Max-Planck-Str. 1, 40237, Düsseldorf, Germany
[c] Bruker AXS GmbH, Östliche Rheinbrückenstraße 49, 76187, Karlsruhe, Germany

ARTICLE INFO

Article history:
Received 10 November 2016
Received in revised form
8 June 2017
Accepted 11 June 2017
Available online 14 June 2017

Keywords:
Co-base superalloys
Atom probe tomography (APT)
High-temperature deformation
X-ray diffraction (XRD)
Phase diagram calculation

ABSTRACT

A γ' strengthened Co–Ti–Cr superalloy is presented with a mass density ~14 % below that of typical Co–Al–W-based alloys. The lattice misfit is sufficiently low to form coherent cuboidal γ' precipitates. Atom probe tomography shows that Cr partitions to the γ phase, but increases the γ' volume fraction compared to a binary Co-Ti alloy to more than 60 %. The solubility of Cr in the γ' phase is significantly higher than expected from previously published values. The γ' solvus temperature is above 1100 °C. The yield strength shows a distinct increase above 600 °C surpassing that of Co–9Al–8W (at.%) and conventional Co-base superalloys, even more so when it is normalized by the mass density.

1. Introduction

Since the re-discovery of a ternary $L1_2$ phase of the type $Co_3(Al,W)$ [1], which was reported for the first time already in 1971 [2], γ' strengthened Co-base superalloys based on the system Co–Al–W have gained renewed worldwide scientific attention [3–7]. While they show very promising mechanical properties [3,8], γ/γ' two phase alloys in the ternary Co–Al–W system suffer from a narrow γ/γ' two-phase region, a low γ' solvus temperature [1], a low phase stability and small solubility for additional alloying elements [9–11] and a high mass density, because of the elevated W-content of 15–30 wt.% (5–12 at.%) that is required to meet the two phase region at the desired phase fractions.

Cobalt is indeed very promising as a base element for high temperature materials as it has a 40 °C higher melting temperature than Ni. Additionally, alloying elements have a lower diffusivity [12] in Co and the lower stacking fault energy might be beneficial for achieving reduced double cross slip rates, higher frequency of strong dislocation locks and thus potentially better creep performance. Furthermore, conventional solid solution and carbide strengthened Co-base superalloys offer superior hot-corrosion resistance to contaminated gas turbine atmosphere environment and exhibit superior thermal fatigue resistance and weldability compared to nickel alloys [13,14]. Therefore, already during the 1960–1970s considerable efforts had been made to identify useful cobalt-base systems, in which γ' hardening might be possible [2,15–18].

The binary Co–Ti system proved to be a promising candidate for that, because a stable γ' Co_3Ti phase exists there, which shows the highest temperature of the maximum flow stress among all the intermetallics with $L1_2$ crystal structure [19]. It was also shown, that binary Co-Ti alloys are superior to binary Ni-Al alloys with a similar γ' volume fraction regarding the flow stress [20]. However, the use of the Co_3Ti phase is hampered by some of its features: according to [21,22], the maximum solubility of Ti in fcc-Co is only ~12 at.%. This content is only sufficient to produce a very low γ' volume fraction of approximately 20 % at 900 °C. Furthermore, the addition of Ni to the Co–Ti system for producing intermediate Co/Ni base superalloys results in the formation of plate-like η precipitates of Ni_3Ti type with $D0_{24}$ crystal structure [23,24]. Additionally, the γ' Co_3Ti phase tends to precipitate discontinuously in an undesirable cellular form, because of a strong change in Ti-solubility with decreasing temperature and a exceedingly high γ/γ' lattice misfit [16,25].

Viatour et al. [26] gave a very comprehensive review on the efforts to produce alloys based on the Co–Ti system. They found that almost all alloying elements they investigated caused a

* Corresponding author.
E-mail address: christopher.zenk@fau.de (C.H. Zenk).

http://dx.doi.org/10.1016/j.actamat.2017.06.024
1359-6454/

formation of additional undesired intermetallic phases such as η-Ni_3Ti ($D0_{24}$), β-Co_3W ($D0_{19}$) or Laves phases at high temperatures. Therefore, they concluded that the use of the Co_3Ti phase is limited to service temperatures below 750 °C. However, they also found that Cr can effectively reduce the γ/γ' lattice misfit and impede discontinuous precipitation reactions at grain boundaries that are detrimental for the mechanical properties. The γ' phase of a Co–10.7Ti–11.0Cr (at.%) alloy (referred to as Co–9Ti–10Cr in their study, as the content is given in wt.%) remained stable even after prolonged aging for 1000 h at 1000 °C. However, they did not include a fully compositionally matured alloy for their structural investigations, as either the Cr content was too low, so that the γ/γ' lattice misfit was not reduced sufficiently or it was too high, which caused the formation of a phase that they termed χ or the Ti content was too high (17.6 at.%) and β-Co_2Ti was formed. Nevertheless, these findings indicate that the Co–Ti–Cr system might indeed serve as a compositional basis for developing promising candidate materials for high temperature applications.

Besides these constitutional considerations γ/γ' Co–Ti–Cr based superalloys might help to reduce the high density of Co–Al–W alloys by means of alloying, while maintaining the positive γ/γ' lattice misfit. As an example, alloys with ~5 wt.% Ti and ~7 wt.% Cr could reduce the mass density of an Co–9Al–8W alloy by more than 7.5 % to 8.5 g/cm^3 which would then be in the range of or even lower than the density of conventional Co-base superalloys without the possibility of γ' strengthening—such as Mar-M509 with 8.85 g/cm^3 [27].

In this study, a Co–11Ti–15Cr γ/γ' superalloy with low mass density is presented and characterized in terms of microstructure, lattice misfit, transformation temperatures, phase compositions and flow stress.

2. Experimental procedures

The Co–11Ti–15Cr alloy (henceforth all compositions are given in at.%), subsequently named CTC-1, was arc-melted under Ar backfilled atmosphere using raw elements of 99.9 % purity. The rod-shaped sample was turned over and re-melted several times to improve compositional homogeneity. The subsequent heat treatment comprised a solution and homogenization step for 100 h at 1150 °C followed by a precipitate aging heat treatment for 100 h at 900 °C. These heat treatments were conducted in one step in a vacuum tube furnace using heating and cooling rates of 5 K min^{-1}. Hereafter this heat treatment is referred to as standard heat treatment. For the atom probe tomography (APT) measurements, a smaller sample was re-heated to 900 °C for about 15 min and quenched in water to avoid γ' precipitation in the matrix channels upon cooling and, therefore, provide compositions characteristic for the aging temperature.

The microstructure was investigated by using scanning electron microscopy (SEM) using a *Zeiss Crossbeam 1540 EsB* in conjunction with a back-scattered electron detector. Prior to microstructural examination, standard sample preparation was conducted, which consisted of grinding by SiC paper up to 4000 grit and polishing using a diamond suspension.

Additionally, transmission electron microscopy (TEM) was carried out in a *Philips CM200* instrument at 200 kV acceleration voltage. The TEM sample was prepared from the standard annealed state. The disc with a diameter of 3 mm was cut to a thickness of ~0.5 mm before mechanically grinding and polishing to a thickness of ~100 μm. The final thinning was performed with a *Struers TenuPol-5* electropolishing unit and *Struers Electrolyte A2*. The electrolyte was cooled to a temperature of −5 to −20 °C using liquid Nitrogen.

The large grain size of several hundred μm in the arc-melted sample impeded powder diffraction experiments, as an insufficient number of grains would contribute to diffraction. As a consequence, to measure the lattice constants of γ and γ', high resolution X-ray diffraction experiments (HRXRD) were carried out at room temperature on a specimen in the standard heat treated state at *Bruker AXS GmbH* in Karlsruhe using a *Bruker D8 DISCOVER* horizontal diffractometer. The instrument was operated using monochromatic $CuK_{\alpha 1}$ radiation and equipped with a energy discriminating *LYNXEYE XE* fast linear detector to cut off the influence of Co fluorescence. Reciprocal Space Maps (RSM) were acquired from an individual grain in the sample around the 001 superlattice reflection of the γ' superstructure and the 002 fundamental reflection which is caused by both γ and γ'. This grain with a suitable orientation with respect to the sample surface (*i.e.* (001) lattice planes as parallel as possible to surface) was identified by looking for the highest intensity in a $\phi - \psi$ scan at the expected 002 Bragg angle 2θ of ~50.6°. Using a series of coupled X-ray tube and detector movements, ω and 2θ were then scanned (each ±1.5°) around the 001 and 002 reflections to record the RSMs. The 002 map was then added up to obtain *intensity vs reciprocal lattice vector* curves consisting of overlapping peaks from the γ and γ' phases. Three pseudo-Voigt functions (a linear combination of Gauss and Lorentz profile) were necessary for fitting the profile to take account for the asymetric peak shape which arises from the difference in the lattice parameters of γ and γ' and the tetragonal distortion of the γ phase due to the coherency stresses [28].

Differential scanning calorimetry (DSC) was performed on the alloy in the heat treated state to determine phase transformation temperatures. Heating and cooling rates of 5 K min^{-1} were used. The characteristic temperatures were determined by averaging the corresponding peak onsets in both the heating and cooling curves.

An isothermal section of the Co–Ti–Cr phase diagram at 900 °C was calculated by the *CALPHAD* method [29] using the *ThermoCalc* software package and the TCNI8 database [30].

Atom probe tomography (APT) samples were prepared from grain interiors using a dual beam FIB system (FEI Helios Nanolab 600/600i) by the conventional liftout technique [31]. For reducing Ga implantation, a low energy (2 keV) Ga beam was used for final shaping of the APT tips. APT analysis was performed using a reflectron equipped local electrode atom probe (*LEAP 3000 XHR, Cameca Instruments*) in pulsed laser mode. The reflectron is a magnetic flight path extension device which increases the spread among neighboring mass-to-charge peaks, hence, enhancing chemical resolution. Using a reflectron substantially improves the precision of chemical analysis in materials containing many related alloying elements [32–35]. Laser pulses of 532 nm wavelength, 12 ps pulse length, 0.4 nJ pulse energy and 200 kHz frequency were applied, while the specimen base temperature was kept at ~40 K. Data reconstruction and analysis was performed using the *Cameca IVAS 3.6.8 software package*. The first ~10^6 ions were not considered for data analysis due to residual Ga ions implanted during FIB milling.

The 0.2 % flow stress was determined from compressive tests at 25 °C, 600 °C, 750 °C, 850 °C, 900 °C, 1000 °C and 1050 °C, and a strain rate of 10^{-4} s^{-1}. For the sake of a better comparison, compression tests on two alloys from Ref. [36], Co–9Al–8W and Co–12Ti (both containing 0.1 at.% B), were conducted also at 850 °C and 1000 °C.

3. Results & discussion

In the following the microstructure parameters of the alloy CTC-1 are presented, before the lattice misfit is discussed on the basis of the HRXRD and TEM investigations. Subsequently the

thermophysical properties and elemental partitioning behavior are addressed before the mechanical properties are compared to other alloys in terms of the compressive yield strength.

3.1. Microstructure

SEM and TEM micrographs of alloy CTC-1 after standard heat treatment are shown in Fig. 1. According to image analysis the γ' precipitates have an average edge length of ~450 nm and occupy a volume fraction of ~66 %.

It was possible to completely solutionize alloy CTC-1, so that no primary precipitates prevailed in the standard heat treated state. Additionally to the γ' precipitates which formed during aging, tiny γ' precipitates were found in the γ channels that formed during the furnace cooling. Neither cellular precipitates nor allotropic transformations were observed, as it was the case in a Co–22Cr–5Ti–1.5Mo alloy reported by Bhowmik et al. [25]. Compared to the ternary Co–9Al–7.5 W alloy presented in Ref. [1], the precipitates have a more cubic morphology indicating a larger lattice misfit. The microstructure of CTC-1 is very similar to the one observed for typical single crystal cast Ni-base superalloys, *i.e.* cubic γ' precipitates with sharp edges and corners and very narrow γ channels between the γ' cubes, in which dislocations would have to squeeze during deformation. In Ref. [36], a binary Co–12Ti alloy was shown to exhibit irregular shaped precipitates after the same aging heat treatment, caused by a too high misfit. This observation indicates that Cr is effective in lowering the γ/γ' lattice misfit of Co–Ti alloys. Apparently a Cr-content of $\gtrapprox$ 10 at.% is necessary in the system Co–Ti–Cr, as an alloy with only 5 at.% Cr still exhibited irregular shaped precipitates, similar to those in binary Co–Ti alloys (also compare micrographs in supplementary material).

3.2. Lattice misfit

This is confirmed by the HRXRD measurements. Fig. 2 shows the reciprocal space map of the 001 γ' superlattice reflection and the 002 fundamental reflection caused by both γ and γ' together with the corresponding summed profiles. Note that Fig. 2a) is magnified by a factor of five with respect to Fig. 2b). Obviously, the distinct broadening of the 002 reflection in both q_z and q_x directions is exclusively caused by the γ phase as the 001 superlattice reflection of the γ' phase is very symmetric. The asymmetry of the 002 reflection directly results from the different lattice parameters of γ' and γ, which correspond to slightly different peak positions of the respective phases with respect to q_z. The portion of the reflection which is caused by γ is asymmetric too, though. This is also an indirect consequence of the difference in the γ and γ' lattice parameters: the γ unit cell is elastically distorted so that the lattice parameter parallel to the γ/γ' interfaces $a_{\gamma,\parallel}$ is strained and approaches the larger γ' lattice parameter, whereas the lattice parameter perpendicular to the interfaces $a_{\gamma,\perp}$ shrinks with respect to its unconstrained state (see also Fig. A.1).

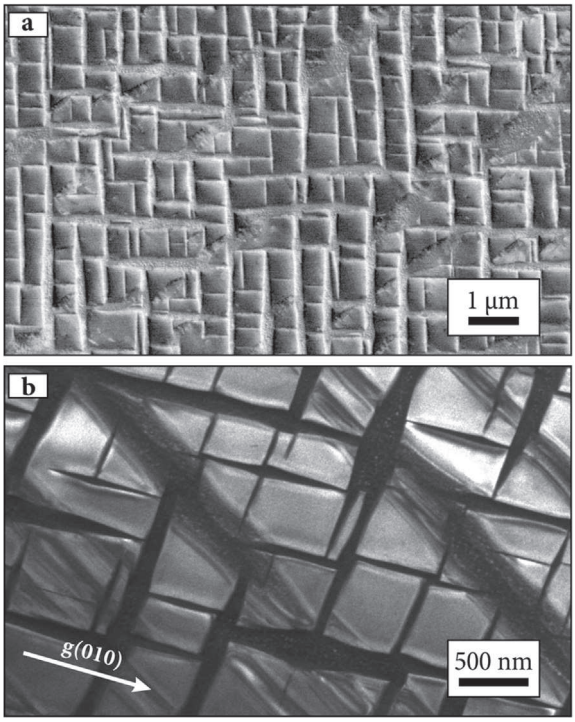

Fig. 1. Microstructure of CTC-1 after aging for 100 h at 900 °C. a) Backscattered electron micrograph, b) TEM dark field image.

In Ref. [36], we had already shown how an equivalent cubic lattice parameter $a_{\gamma,cub}$ for the γ phase can be estimated under the assumption of isotropic material behavior. Equation (A.4) is an extension of this procedure which uses all the elastic constants of the matrix phase or an approximation for them. For details see Appendix A. A magnified version of the 002 diffraction profile with a linear scale can be found in Fig. 3. It is observed that the lattice parameter of γ' is 3.5892 Å ($q_z(\gamma') = 5.5722\ \mathrm{nm}^{-1}$) and, using the elastic constants for fcc Co taken from Ref. [37], the equivalent cubic lattice parameter $a_{\gamma,cub}$ is 3.5700 Å ($q_z(\gamma_\perp) = 5.6341\ \mathrm{nm}^{-1}$, $q_z(\gamma_\parallel) = 5.5801\ \mathrm{nm}^{-1}$). The γ/γ' lattice misfit δ can then be calculated by

$$\delta = 2 \cdot \frac{a_{\gamma'} - a_{\gamma,cub}}{a_{\gamma'} + a_{\gamma,cub}} \tag{1}$$

and is found to be 0.54 % for alloy CTC-1. This value is very close to the 0.53 % which was reported for a Co–9.2Al–9W alloy by Sato et al. [1]. Compared to binary Co–Ti alloys, which were reported to have a lattice misfit of 0.75–1.67 % [26,36], δ of the present alloy CTC-1 was significantly reduced, so that cubic shaped γ' precipitates can form. The observation that Cr is effective in reducing the lattice misfit of Co–Ti alloys is in consistence with the findings reported in Ref. [26]. However, their results suggest that the addition of Cr is even more effective in reducing the lattice misfit than what is found in this study. A lattice misfit of 0.54 % would probably still be considered too high in the case of Ni-base superalloys, which typically exhibit values of ~–0.1 %. Nevertheless, the γ' morphology in CTC-1 is cubic and the γ and γ' peaks in Figs. 2b) and 3 are not separated, but still very continuous, which indicates a high degree of coherency.

Another indicator for coherent γ/γ' interfaces is the large width of the 002 reflection with respect to q_x in Fig. 2b): this corresponds to strongly tilted or bent γ lattice planes close to the γ/γ' interface. If the precipitates were incoherent a) the separation of the γ' and γ peaks would be more distinct, b) the tetragonal distortion of the γ matrix phase would not be present, *i.e.* the corresponding reflection would be symmetric in terms of q_z and c) the width of the γ peak with respect to q_x would be smaller (similar to the γ' superlattice reflection in Fig. 2a) as no bending of lattice plane was to be expected.

To confirm that the γ/γ' interfaces are coherent, TEM investigations in conditions in which interfacial dislocations should be visible were performed. Two of the acquired bright field images obtained in the same grain in two perpendicular two beam conditions are shown in Fig. 4. No misfit dislocations could be found in

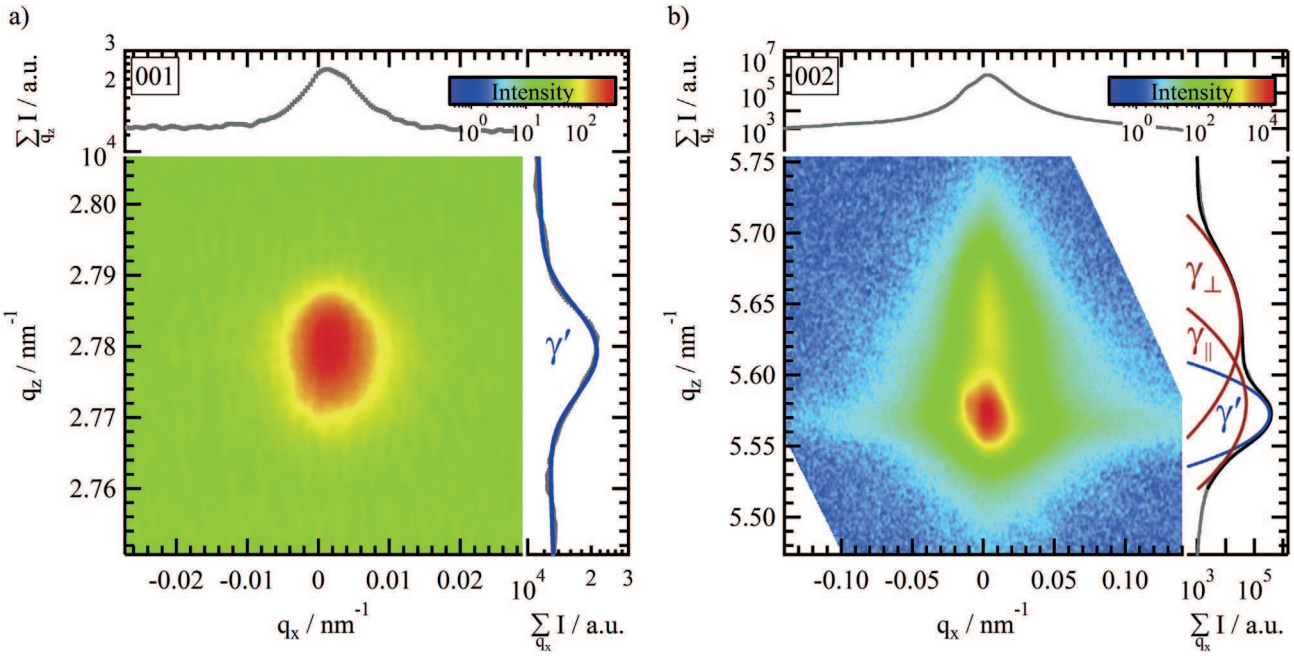

Fig. 2. High resolution X-ray diffraction results. Reciprocal space mapping of a) the γ′ 001 superlattice reflection and b) the γ/γ′ 002 fundamental reflection. Additionally, the logarithm of the summed up intensities over q_x and q_z is included.

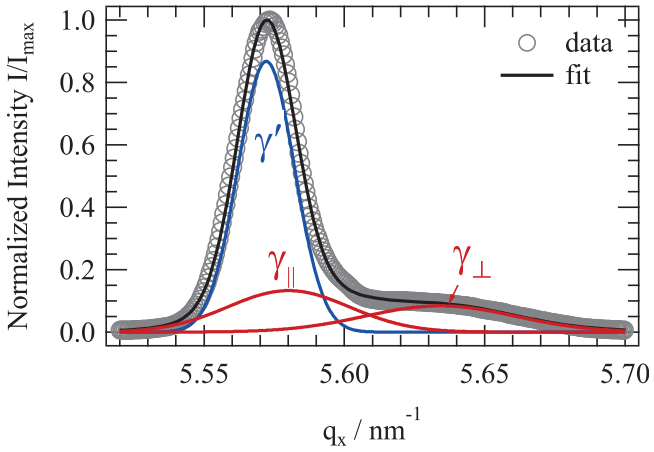

Fig. 3. Diffraction profile obtained by adding up the 002 reciprocal space map over q_z.

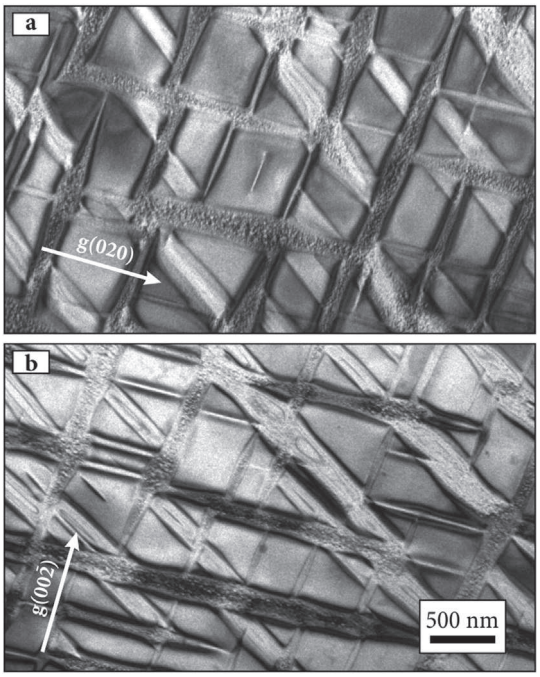

Fig. 4. TEM bright field micrographs of the standard annealed state taken near the [100] zone axis in two beam conditions in which potential misfit dislocations should be visible: a) g(020), b) g(00$\bar{2}$).

the present sample. The two images were taken near the [100] zone axis. However, the observations did not change when the sample was tilted further away from the zone axis. The conclusion that coherency is still given despite a comparatively high lattice misfit is conceivable due to two reasons: Positive misfit alloys typically show a decrease of δ with increasing temperature, *i.e.* δ would be smaller than 0.54 % at the aging temperature of 900 °C. This is contrary to negative misfit alloys (which includes the most Ni-base alloys) where δ usually gets even more negative with increasing temperature.

Another reason for coherent precipitates despite a comparatively high lattice misfit could arise from a difference in elastic properties. Fig. 5 illustrates the Young's modulus of fcc-Co and fcc-Ni in the different crystallographic directions. It is evident that both crystals show a similar elastic anisotropy. Ni is elastically stiffer than Co in all directions. As a consequence, the stresses $\sigma_{\parallel}$ that are caused by a certain lattice misfit in Ni are higher than the ones that would form in Co. Equation (A.7) can be used to estimate these stresses. In the present alloy CTC-1 these stresses amount to 625 MPa (using the elastic constants for fcc Co from Ref. [37]). The same degree of tetragonal distortion in Ni would involve misfit stresses of 955 MPa (using the elastic constants for fcc Ni from Ref. [38]). This observation indicates that the lattice misfit that Co-base superalloys can bear without losing coherency could be higher than the one in Ni-base superalloys. It would also imply that the

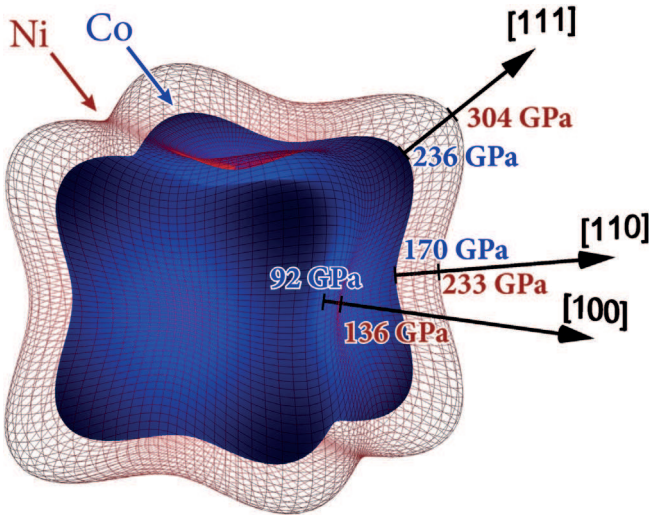

Fig. 5. Surface representing the Young's modulus of Co (inner blue solid) and Ni (outer red mesh) in different crystallographic directions calculated using the elastic constants of fcc-Co [37] and fcc-Ni [38]. (For interpretation of the references to colour in this figure legend, the reader is referred to the web version of this article.)

optimum lattice misfit for achieving the best properties would be different for Co-base alloys.

3.3. Thermophysical properties

The DSC measurements on the heat treated state revealed that the γ' solvus temperature is 1135 °C, *i.e.* it is by ~150 °C higher than in comparable Co–Al–W alloys [1,36]. However, the solidus (1153 °C) and liquidus temperatures (1327 °C) are by far lower. A ternary Co–9Al–8W alloy for instance has solidus and liquidus temperatures of 1446 °C and ~1460 °C respectively [36]. As reported in Ref. [36], a binary Co–12Ti alloy has a γ' solvus temperature of 1022 °C and a melting range of 1217–1337 °C, *i.e.* the addition of Cr caused an increase of the γ' solvus, but a decrease of the solidus and liquidus temperatures. Similar to the Co-Ge-W alloys discussed in Ref. [39] and analogue to the Ni-Ge system discussed in Ref. [40], the low melting temperatures of alloy CTC-1 in combination with the ability to form γ' precipitates could be exploited for potential braze alloys for Co-base superalloys.

The aforementioned binary Co–12Ti alloy only exhibited a γ' volume fraction of approximately 20 %, *i.e.* the addition of Cr also increased the percentage of γ' significantly to more than ~60 %. Alloys that contained 5 and 10 at.% Cr, contained γ' fractions of ~30 and ~45 % respectively. SEM micrographs of these alloys can be found in the supplementary material.

3.4. Phase composition

For better understanding why the addition of Cr leads to such an increase of the γ' volume fraction APT measurements were conducted. The reconstruction of the data for Cr is shown in an atom map in Fig. 6a. A 9.6 at.% Ti iso concentration surface is included to visualize the γ/γ' interface. We observe that Cr is enriched inside the γ phase. The concentration profile in Fig. 6b was obtained using proximity histograms for the denoted isoconcentration surface. It is evident that Ti is strongly enriched in the γ' phase, whereas Cr preferentially partitions into the γ phase. The phase compositions were measured in subvolumes at least 5 nm distant from the interface and containing at least ~10^6 atoms. They are given in Table 1 together with the respective nominal composition c_0. The γ'

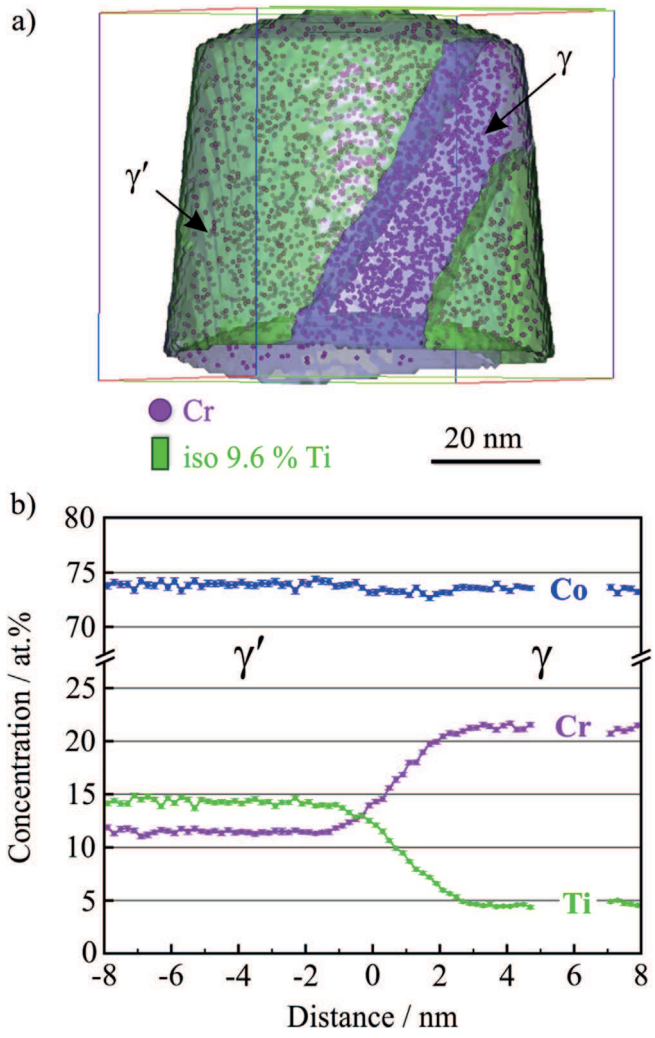

Fig. 6. (a) Atom probe tomography elemental map and (b) corresponding concentration profile across the γ/γ' interface.

phase approximates a $Co_3(Ti,Cr)$ stoichiometry, suggesting that Cr occupies the Ti sublattice in Co_3Ti.

To the authors' knowledge, the only work on phase diagrams and reactions in the Co-rich corner of the Co–Ti–Cr ternary system [41] is based on old and partly contradicting studies [42,43]: According to [42], the present composition Co–11Ti–15Cr is situated in a $\gamma + \lambda_3$ or two-phase region, where λ_3 is a C14 Laves phase. However, apart from γ and γ' no further intermetallic phases were found in the present alloy CTC-1. Reference [43] correctly suggests a γ/γ' two-phase region (γ' is designated ϕ in their work), though their data were assessed at 1000 °C.

To check the applicability of current databases on the Co–Ti–Cr system, a 900 °C isothermal section of the ternary phase diagram was calculated using the TCNI 8 database (see Fig. 7). Additionally,

Table 1
Nominal composition c_0, γ/γ' compositions c_γ and $c_{\gamma'}$ as measured by APT (in at.%) and elemental partitioning coefficient $k_i^{\gamma'/\gamma}$.

	c_0/at.%	c_γ/at.%	$c_{\gamma'}$/at.%	$k_i^{\gamma'/\gamma}$
Co	74	72.7	74.6	1.03
Ti	11	5.1	14.1	2.76
Cr	15	22.2	11.3	0.51

the nominal composition of CTC-1, the measured composition of γ and γ′, and the corresponding tie-line are included in the diagram. It can be seen that the solubility of Cr in the γ′ phase is strongly underestimated by the calculation. Also in Ref. [44] a Cr-solubility of <4.5 at.% was found as compared to the 11.3 at.% which was observed in this study. However, the data reported in the earlier publication were acquired from a sample that had been aged at 1050 °C for 48 h which somewhat restricts comparability. The thermodynamic calculation shown in Fig. 7 also predicts a C15 Laves phase to be stable for the given composition at an aging temperature of 900 °C, which was not experimentally observed in our current study.

It could be argued that the microstructure and APT investigations were not performed in thermodynamic equilibrium. However, even after aging the alloy for 500 h at 900 °C – which corresponds to a very high homologous temperature of ~ 0.8 T_m – no additional phases were observed. This fact and the coarsened precipitates observed after the relatively long aging time of 500 h both suggest that γ and γ′ may actually form a two-phase equilibrium in this alloy at 900 °C. Micrographs of the long term aged state can be found in the supplementary material.

The mole fraction of γ′ can be calculated from the phase compositions by using the lever rule based on the mass balance equation

$$\vec{c}_0 = (1 - f_m)\cdot\vec{c}_\gamma + f_m\cdot\vec{c}_{\gamma'} \quad (2)$$

where f_m is the γ′ mole fraction. As the difference in atomic densities between γ and γ′ is marginal, f_m equals the γ′ volume fraction f_v. In Equation (2) the compositions of the compound ($\vec{c}_0$) and the individual phases ($\vec{c}_\gamma$, $\vec{c}_{\gamma'}$) are represented as vectors in compositional space, *i.e.* they contain the concentration c_i of the individual elements *i* as entries. Transposing the equation gives

$$(\vec{c}_0 - \vec{c}_\gamma) = f_m\cdot(\vec{c}_{\gamma'} - \vec{c}_\gamma) \quad (3)$$

i.e. if $(c_{i,0} - c_{i,\gamma})$ is plotted versus $(c_{i,\gamma'} - c_{i,\gamma})$ and linear regression is performed, the slope provides the fraction of γ′. For alloy CTC-1, this method gives $f_v \approx f_m = (66.0\pm0.8)$ %, which is in perfect agreement with image analysis.

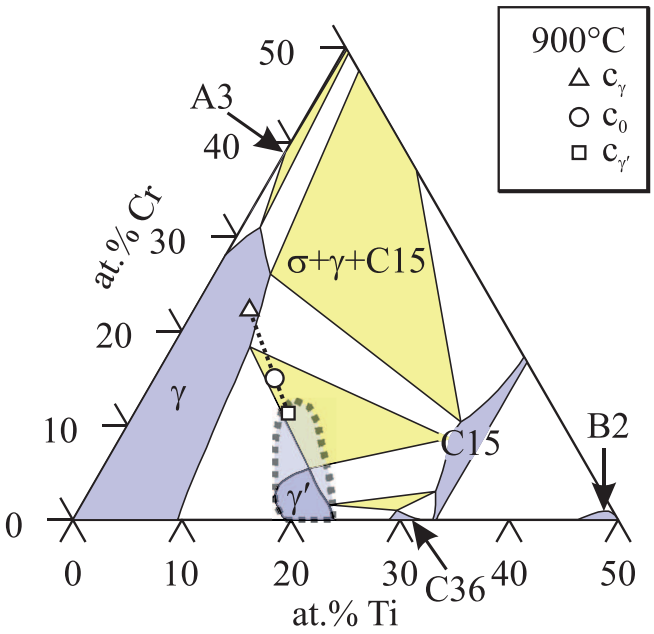

Fig. 7. Calculated isothermal section of the Co–Ti–Cr phase diagram at 900 °C including nominal alloy composition and measured compositions of γ and γ′ (open symbols), which indicate a larger γ′ single phase region (dashed line).

A customary measure for the preferential enrichment of a certain element i in γ or γ′ is the elemental partitioning coefficient $k_i^{\gamma'/\gamma} = c_{i,\gamma'}/c_{i,\gamma}$, which is also included in Table 1. It is found that the partitioning behavior of Ti and Cr in this alloy system is not as pronounced as it is observed in Ni-base superalloys. In Ref. [45] the partitioning behavior of different elements in typical Ni-base superalloys has been summarized. The partitioning coefficient $k_{Cr}^{\gamma'/\gamma}$ was found to be around 0.2 and $k_{Ti}^{\gamma'/\gamma} \approx 6$, *i.e.* the preferential partitioning of these elements is more than twice as pronounced compared to the present alloy CTC-1. However, values almost identical to the ones observed in this study have been reported for Co–Al–W based alloys, where $k_{Cr}^{\gamma'/\gamma} \approx 0.57$ [46] and $k_{Ti}^{\gamma'/\gamma} \approx 2.5$ [47].

As a summary, it can be stated that the addition of Cr at the expense of Co increases the γ′ volume fraction despite its preferential partitioning into the γ phase. This was also found for Co–Al–W base alloys [46].

3.5. Mechanical properties

The mechanical properties in terms of the flow stress are shown in Fig. 8. A distinct increase of the flow stress of alloy CTC-1 above 600 °C is observed. This is contrary to results reported in Ref. [26], where no anomalous increase in flow strength was found for Co–Ti–Cr alloys. Furthermore these authors detected that the addition of Cr causes a decrease in yield strength, whereas in the current study a strong increase is found compared to a Co–12Ti alloy. The inferior yield strength they observed might be due to the different heat treatment or be caused by an overly high Cr content of 17.4–21.8 at.% which in turn might favor the formation of additional intermetallic phases (*e.g.* χ), discontinuous coarsening or an allotropic transformation as observed by Bhowmik et al. for a Mo-containing but otherwise very similar alloy [25]. Unfortunately the structural and mechanical characterization in Ref. [26] were not conducted on the same alloys, which impedes the identification of the most likely reason for the observed difference.

Additionally, Fig. 8 shows that the yield strength of a conventional carbide and solid solution strengthened Co-base superalloy *Mar-M 509* (Co–3C–0.25Ti–27.1Cr–10.2Ni–0.3Zr–1.2Ta–2.3 W) is surpassed by CTC-1 over the whole temperature range. The flow stress of alloy CTC-1 is in the same range as that of a Co-9Al-8W alloy, though the peak strength of the flow stress is seemingly shifted towards slightly higher temperatures. As seen in 8b), the mechanical response of alloy CTC-1 is even better, if the strength is normalized by the alloy density (CTC-1: 8.10 g/cm^3, Co–9Al–8W: 9.45 g/cm^3, Co–12Ti: 8.30 g/cm^3, Mar-M 509: 8.85 g/cm^3 [27]) and is superior to the properties of the other alloys included here over the whole temperature range.

If there is a continuous γ/γ′ two-phase region between Co–Co_3(Al,W) and Co–Co_3(Ti,Cr), the two γ′ strengthened alloying systems might well complement each other. In Co–Al–W alloys, the substitution of Al and W by Ti and Cr (in certain ratios) might help to increase the γ′ solvus temperature and volume fraction, reduce the mass density and shift the yield strength towards higher temperatures while maintaining a sufficiently high solidus temperature. Additionally it might be possible to include Cr in γ′ strengthened Co-base superalloys without adding Ni, which is not possible in Co–Al–W alloys, because other phases form at the expense of γ/γ′ [11,48]. However, it might nontheless be of interest to investigate such alloys, because in that way the positive misfit can be retained, while it strongly decreases when Ni is added

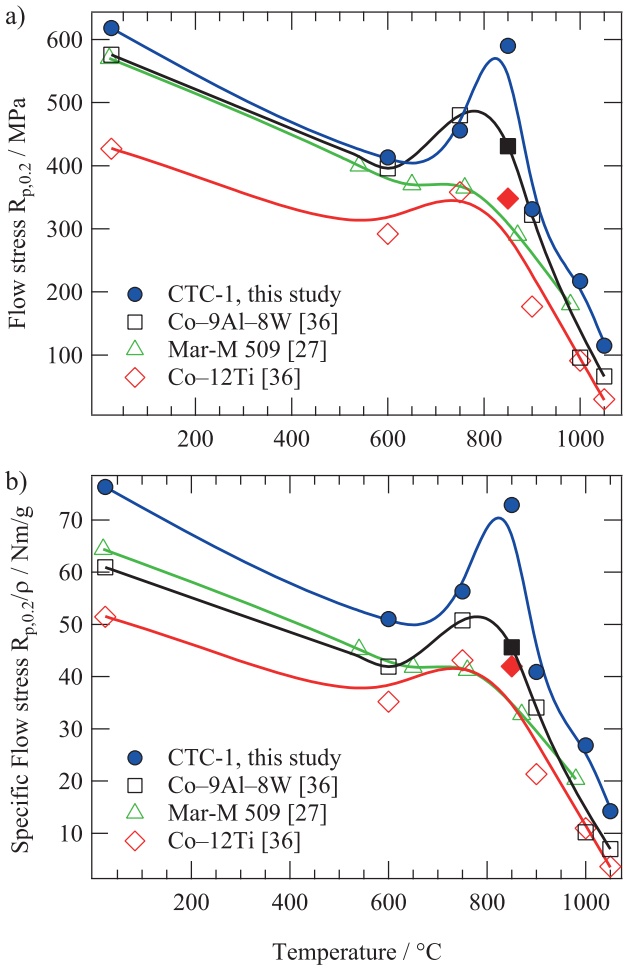

Fig. 8. Comparison of the a) yield strength and b) density normalized yield strength versus temperature curves of CTC-1 (Co–11Ti–15Cr), Co–9Al–8W, Mar-M 509 (Co–3C–0.25Ti–27.1Cr–10.2Ni–0.3Zr–1.2Ta–2.3 W) and Co–12Ti, including data from Refs. [27,36]. Compositions are given in at.%.

[46,48]. The positive misfit in turn might be beneficial for the creep properties [49,50]. Additionally it might be of advantage, because according to [51] the addition of Ni to Co-base alloys is accompanied by a decrease of the anti phase boundary and superlattice intrinsic stacking fault energies.

4. Summary & conclusions

A γ' strengthened, low-density Co–11Ti–15Cr superalloy CTC-1 with a γ' solvus temperature above 1100 °C is presented. It was found that by the addition of Cr, the γ/γ' lattice misfit can be reduced sufficiently (0.54 %) to form an advantageous cubic precipitate morphology and coherent interfaces. The lower elastic stiffness of Co as compared to Ni increases the maximum tolerable and also the optimal γ/γ' lattice misfit for Co-base superalloys compared to in Ni-base superalloys.

Despite preferential partitioning of Cr into the γ phase, it increases the γ' volume fraction to more than 60 %. The solubility of Cr in the γ' phase is significantly higher than previously published data show. The alloy's yield strength shows a distinct increase above 600 °C and surpasses the one of Co–9Al–8W, even more so when normalized by mass density (9.4 g/cm^3 for Co–9Al–8W, 8.1 g/cm^3 for the new alloy presented here).

Acknowledgements

The authors acknowledge funding by the Deutsche Forschungsgemeinschaft (DFG) through projects B3 and A4 of the Collaborative Research Center SFB/TR 103.

Appendix A. Coherency Stresses and Tetragonal Distortion

A schematic of the interfacial stresses and the tetragonal distortion is shown in Figure A.1. The strain state in dependence of the stress is described by

$$\varepsilon_{ij} = S_{ijkl}\sigma_{kl} \tag{A.1}$$

where S_{ijkl} is the elastic compliance tensor.

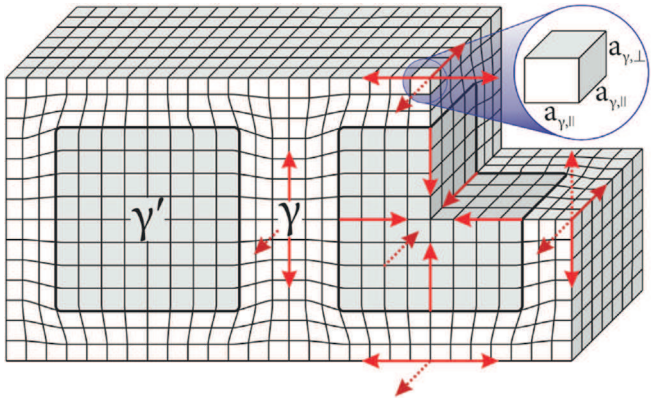

Fig. A.1. Schematic of coherency stresses and tetragonal distortion of the γ matrix phase.

The peak fitting above gives the lattice constant of the γ' phase and the two lattice parameters of the tetragonal distorted γ phase $a_{\gamma,\parallel}$ and $a_{\gamma,\perp}$. Assuming plane stress in the matrix, *i.e.* no stresses perpendicular to the interfaces ($\sigma_{11} = \sigma_{22} = \sigma_{\parallel}$, $\sigma_{33} = \sigma_{\perp} = 0$) gives

$$\varepsilon_{\parallel} = \sigma_{\parallel}(S_{11} + S_{12}) = \frac{a_{\gamma,\parallel} - a_{\gamma,cub}}{a_{\gamma,cub}} \tag{A.2}$$

and

$$\varepsilon_{\perp} = 2\sigma_{\parallel}S_{12} = \frac{a_{\gamma,\perp} - a_{\gamma,cub}}{a_{\gamma,cub}} \tag{A.3}$$

for the strain parallel ($\varepsilon_{\parallel}$) and perpendicular ($\varepsilon_{\perp}$) to the interfaces. The equivalent cubic lattice parameter $a_{\gamma,cub}$ can be obtained by dividing Equation (A.3) by Equation (A.2) and solving for $a_{\gamma,cub}$:

$$a_{\gamma,cub} = \frac{(S_{11} + S_{12})a_{\gamma,\perp} - 2S_{12}a_{\gamma,\parallel}}{S_{11} - S_{12}} \tag{A.4}$$

Thus, the coherency stresses $\sigma_{\parallel}$ can be calculated directly using Equation (A.2) or (A.3) or from the degree of tetragonal distortion R:

$$R = \frac{a_{\gamma,\parallel}}{a_{\gamma,\perp}} = \frac{a_{\gamma,cub}\left(1 + \varepsilon_{\parallel}\right)}{a_{\gamma,cub}(1 + \varepsilon_{\perp})} = \frac{1 + \varepsilon_{\parallel}}{1 + \varepsilon_{\perp}} \tag{A.5}$$

Adding 1 to Equations (A.2) and (A.3) and dividing the former by the latter equals Equation (A.5):

$$R = \frac{1 + \varepsilon_{\parallel}}{1 + \varepsilon_{\perp}} = \frac{\sigma_{\parallel}(S_{11} + S_{12}) + 1}{2\sigma_{\parallel}S_{12} + 1} \tag{A.6}$$

Solving this for $\sigma_{\parallel}$ gives the magnitude of the coherency stresses

in the γ channels in dependence of tetragonal distortion and elastic constants:

$$\sigma_{\parallel} = \frac{1 - R}{2RS_{12} - S_{12} - S_{11}} \quad \text{(A.7)}$$

Appendix B. Supplementary data

Supplementary data related to this article can be found at http://dx.doi.org/10.1016/j.actamat.2017.06.024.

References

[1] J. Sato, T. Omori, K. Oikawa, I. Ohnuma, R. Kainuma, K. Ishida, Cobalt-base high-temperature alloys, Science 312 (2006) 90–91.
[2] C.S. Lee, Precipitation-hardening Characteristics of Ternary Cobalt - Aluminum - X Alloys (Ph.D. thesis), The University of Arizona, 1971.
[3] A. Bauer, S. Neumeier, F. Pyczak, M. Göken, Microstructure and creep strength of different γ/γ'-strengthened Co-base superalloy variants, Scr. Mater. 63 (2010) 1197–1200.
[4] T.M. Pollock, J. Dibbern, M. Tsunekane, J. Zhu, A. Suzuki, New Co-based γ-γ' high-temperature alloys, JOM 62 (2010) 58–63.
[5] H.Y. Yan, V.A. Vorontsov, J. Coakley, N.G. Jones, H.J. Stone, D. Dye, Quaternary alloying effects and the prospects for a new generation of Co-Base superalloys, in: E.S. Huron, R.C. Reed, M.C. Hardy, M.J. Mills, R.E. Montero, P.D. Portella, J. Telesman (Eds.), Superalloys 2012, John Wiley and Sons, 2012, pp. 705–714.
[6] K. Tanaka, H. Inui, Effects of alloying elements on physical and mechanical properties of Co-Al-W-Based $L1_2$/fcc two-phase alloys, Mater. Sci. Forum 783–786 (2014) 1195–1200.
[7] A. Suzuki, H. Inui, T.M. Pollock, $L1_2$-Strengthened cobalt-base superalloys, Annu. Rev. Mater. Res. 45 (2015) 345–368.
[8] A. Suzuki, T. Pollock, High-temperature strength and deformation of γ/γ' two-phase Co-Al-W-base alloys, Acta Mater. 56 (2008) 1288–1297.
[9] Y. Tsukamoto, S. Kobayashi, T. Takasugi, The stability of γ'-Co_3(Al,W) phase in Co-Al-W ternary system, Mater. Sci. Forum 654–656 (2010) 448–451.
[10] S. Kobayashi, Y. Tsukamoto, T. Takasugi, The effects of alloying elements (Ta, Hf) on the thermodynamic stability of γ'-Co_3 (Al,W) phase, Intermetallics 31 (2012) 94–98.
[11] A. Bauer, S. Neumeier, F. Pyczak, M. Göken, Creep strength and microstructure of polycrystalline γ'-strengthened Cobalt-base superalloys, in: E.S. Huron, R.C. Reed, M.C. Hardy, M.J. Mills, R.E. Montero, P.D. Portella, J. Telesman (Eds.), Superalloys 2012, TMS, John Wiley & Sons, Warrendale, PA, 2012, pp. 695–703.
[12] S. Neumeier, H.U. Rehman, J. Neuner, C.H. Zenk, S. Michel, S. Schuwalow, J. Rogal, R. Drautz, M. Göken, Diffusion of solutes in fcc cobalt investigated by diffusion couples and first principles kinetic Monte carlo, Acta Mater 106 (2016) 304–312.
[13] A.M. Beltran, Co-base alloys, in: C.T. Sims, N.S. Stoloff, W.C. Hagel (Eds.), Superalloys II, John Wiley & Sons, Inc., 1987, pp. 135–164.
[14] T.M. Pollock, Alloy design for aircraft engines, Nat. Mater. 15 (2016) 809–815.
[15] J.M. Drapier, J. de Brouwer, D. Coutsouradis, Refractory metals and intermetallic precipitates in cobalt-chromium alloys, Kobalt 27 (1965) 55–66.
[16] C. Rogister, D. Coutsouradis, L. Habraken, Verbesserung hitzebeständiger Kobaltlegierungen durch Aushärtung, Kobalt 34 (1967) 3–8.
[17] J.M. Drapier, D. Coutsouradis, Aushärtung von Kobalt-Chrom-Tantal-Legierungen, Kobalt 39 (1968) 55–64.
[18] J. Blaise, P. Viatour, J.M. Drapier, Über Stabilität und Ausscheidung der Co_3Ti-Phase in Kobalt-Titan-Legierungen, Kobalt 49 (1970).
[19] D.-M. Wee, O. Noguchi, Y. Oya, T. Suzuki, New $L1_2$ ordered alloys having the positive temperature dependence of strength, Trans. Jpn. Inst. Metals 21 (1980) 237–247.
[20] M. N. Thompson, J. W. Edington, High temperature mechanical properties and deformation modes in a precipitation hardened Co-Ti alloy, in: Proc. 2nd Int. Conf. Strength of Metals and Alloys, vol. 3, pp. 1150–1154.
[21] J.L. Murray, The Co-Ti (Cobalt-Titanium) system, Bull. Alloy Phase Diagr. 3 (1982) 74–85.
[22] J.L. Murray, Phase Diagrams of Binary Titanium Alloys, ASM International, Materials Park, OH, 1987.
[23] P. Viatour, J.M. Drapier, D. Coutsouradis, L. Habraken, Gefüge und Eigenschaften von CM-7, einer schmied- und aushärtbaren Kobaltlegierung, Kobalt 51 (1971) 61–68.
[24] C. Cui, D. Ping, Y. Gu, H. Harada, A new Co-Base superalloy strengthened by γ' phase, Mater. Trans. 47 (2006) 2099–2102.
[25] A. Bhowmik, S. Neumeier, S. Rhode, H.J. Stone, Allotropic transformation induced stacking faults and discontinuous coarsening in a γ-γ' Co-base alloy, Intermetallics 59 (2015) 95–101.
[26] P. Viatour, J.M. Drapier, D. Coutsouradis, Stability of the γ'-Co_3 Ti compound in simple and complex cobalt alloys, Cobalt 3 (1973) 67–74.
[27] J.R. Davis (Ed.), ASM Specialty Handbook: Nickel, Cobalt, and Their Alloys, ASM International, Materials Park, OH 44073, 2000.
[28] H.-A. Kuhn, H. Biermann, T. Ungar, H. Mughrabi, An X-ray study of creep-deformation induced changes of the lattice mismatch in the γ'-hardened monocrystalline Nickel-base superalloy SRR 99, Acta Metall. Mater. 39 (1991) 2783–2794.
[29] H.L. Lukas, S.G. Fries, B. Sundman, Computational Thermodynamics - the CALPHAD Method, Cambridge University Press, Shaftesbury Road, Cambridge, CB2 8BS, UK, 2007.
[30] J.O. Andersson, T. Helander, L. Höglund, P.F. Shi, B. Sundman, Thermo-Calc, DICTRA, Computational tools for materials science, CALPHAD 26 (2002) 273–312.
[31] K. Thompson, D. Lawrence, D. Larson, J. Olson, T. Kelly, B. Gorman, In situ site-specific specimen preparation for atom probe tomography, Ultramicroscopy 107 (2007) 131–139.
[32] K. Matuszewski, R. Rettig, H. Matysiak, Z. Peng, I. Povstugar, P. Choi, J. Müller, D. Raabe, E. Spiecker, K. Kurzydłowski, R. Singer, Effect of Ruthenium on the precipitation of topologically close packed phases in Ni-based superalloys of 3rd and 4th generation, Acta Mater. 95 (2015) 274–283.
[33] A. Parsa, P. Wollgramm, H. Buck, C. Somsen, A. Kostka, I. Povstugar, P.-P. Choi, D. Raabe, A. Dlouhy, J. Müller, E. Spiecker, K. Demtroder, J. Schreuer, K. Neuking, G. Eggeler, Advanced scale bridging microstructure analysis of single crystal Ni-base superalloys, Adv. Eng. Mater. 17 (2015) 216–230.
[34] Z. Peng, I. Povstugar, K. Matuszewski, R. Rettig, R. Singer, A. Kostka, P.-P. Choi, D. Raabe, Effects of Ru on elemental partitioning and precipitation of topologically close-packed phases in Ni-based superalloys, Scr. Mater. 101 (2015) 44–47.
[35] D. Tytko, P.-P. Choi, J. Klöwer, A. Kostka, G. Inden, D. Raabe, Microstructural evolution of a Ni-based superalloy (617B) at 700 °C studied by electron microscopy and atom probe tomography, Acta Mater. 60 (2012) 1731–1740.
[36] C.H. Zenk, S. Neumeier, H.J. Stone, M. Göken, Mechanical properties and lattice misfit of γ/γ' strengthened Co-base superalloys in the Co–W–Al–Ti quaternary system, Intermetallics 55 (2014) 28–39.
[37] J. Gump, H. Xia, M. Chirita, R. Sooryakumar, M.A. Tomaz, Elastic constants of face-centered-cubic cobalt, J. Appl. Phys. 86 (1999) 6005.
[38] C. Kittel, Introduction to Solid State Physics, eighth ed., Wiley, 2005.
[39] C. Zenk, A. Bauer, P. Goik, S. Neumeier, H. Stone, M. Göken, Microstructure, lattice misfit, and high-temperature strength of γ'-strengthened Co-Al-W-Ge model superalloys, Metallurgical Mater. Trans. A Phys. Metallurgy Mater. Sci. 47 (2016) 2141–2149.
[40] M.K. Dinkel, P. Heinz, F. Pyczak, A. Volek, M. Ott, E. Affeldt, A. Vossberg, M. Göken, R.F. Singer, New boron and silicon free single crystal-diffusion brazing alloys, in: R. Reed, K. Green, P. Caron (Eds.), Superalloys 2008, TMS, Warrendale, PA, 2008, pp. 211–220.
[41] K.P. Gupta, The Co-Cr-Ti system (Cobalt-Chromium-Titanium), J. Phase Equilibria 22 (2001) 52–60.
[42] B.G. Livshits, Y.D. Khorin, J. Inorg. Chem. 3 (1958) 193–205.
[43] E.K. Zakharov, B.G. Livshits, Izv. Vyssh. Ucheb. Zaved, Chern. Met. 11 (1960) 105–112.
[44] Y. Liu, T. Takasugi, O. Izumi, Alloying behavior of Co_3Ti, Metall. Trans. A 17A (1986) 1433–1439.
[45] F. Pyczak, B. Devrient, H. Mughrabi, The effects of different alloying elements on the thermal expansion coefficients, lattice constants and misfit of nickel-based superalloys investigated by X-ray diffraction, in: K.A. Green, T.M. Pollock, H. Harada, T.E. Howson, R.C. Reed, J.J. Schirra, S. Walston (Eds.), Superalloys 2004, TMS (The Minerals, Metals & Materials Society), Warrendale, PA, 2004, pp. 827–836.
[46] I. Povstugar, C.H. Zenk, R. Li, P.-P. Choi, S. Neumeier, O. Dolotko, M. Hoelzel, M. Göken, D. Raabe, Elemental partitioning, lattice misfit and creep behaviour of Cr containing γ' strengthened Co base superalloys, Mater. Sci. Technol. 32 (2016) 220–225.
[47] I. Povstugar, P.-P. Pyuck, S. Neumeier, A. Bauer, C.H. Zenk, M. Göken, D. Raabe, Elemental partitioning and mechanical properties of Ti- and Ta-containing Co–Al–W-base superalloys studied by atom probe tomography and nanoindentation, Acta Mater. 78 (2014) 78–85.
[48] C.H. Zenk, S. Neumeier, N.M. Engl, S.G. Fries, O. Dolotko, M. Weiser, S. Virtanen, M. Göken, Intermediate Co/Ni-Base model superalloys - thermophysical properties, creep and oxidation, Scr. Mater. 112 (2016) 83–86.
[49] H. Mughrabi, The importance of sign and magnitude of γ/γ' lattice misfit in superalloys–with special reference to the new γ'-hardened cobalt-base superalloys, Acta Mater 81 (2014) 21–29.
[50] M. Titus, A. Suzuki, T. Pollock, Creep and directional coarsening in single crystals of new γ–γ' Cobalt-base alloys, Scr. Mater. 66 (2012) 574–577.
[51] M.S. Titus, Y.M. Eggeler, A. Suzuki, T.M. Pollock, Creep-Induced planar defects in $L1_2$-containing Co- and CoNi-base single-crystal superalloys, Acta Mater. 82 (2015) 530–539.